International Journal of Mass Spectrometry 288 (2009) 22–35

Contents lists available at ScienceDirect

International Journal of Mass Spectrometry

journal homepage: www.elsevier.com/locate/ijms

Condensation reaction of $C_4H_4^+$ with pyridine

C.Q. Jiao[a], J.A. Boatz[b], C.A. DeJoseph Jr.[c], A. Garscadden[c,*]

[a] Innovative Scientific Solutions Inc., Dayton, OH 45440, USA
[b] Air Force Research Laboratory, Edwards AFB, CA 93524, USA
[c] Air Force Research Laboratory, Wright-Patterson AFB, OH 45433, USA

ARTICLE INFO

Article history:
Received 7 April 2009
Received in revised form 17 July 2009
Accepted 21 July 2009
Available online 29 July 2009

Keywords:
Proton transfer
Charge transfer
Condensation
Isotope effect
GAMESS

ABSTRACT

$C_4H_4^+$ reacts with pyridine (C_5H_5N) via the channels of proton transfer, charge transfer and condensation with H-elimination. The condensation reaction is of general interest in terms of basic chemistry and is the focus of the present study. By means of theoretical calculations and Fourier transform mass spectrometer experiments using deuterated pyridine and substituted pyridines, the structure of the product ion and the reaction pathways are investigated. From the experimental results we find that the H atom that is eliminated can originate from either pyridine or $C_4H_4^+$. The experiments show that elimination of an H atom from $C_4H_4^+$ is preferred and that there is an observable kinetic isotope effect. By replacing H atoms with methyl groups in *ortho* positions of pyridine, the experimental results also suggest possible steric blocking to the condensation. Based on the experimental observations and results of theoretical calculations of several possible structures of intermediates, transition states, and final product ions, a possible reaction scheme for the condensation-H-elimination is discussed.

Published by Elsevier B.V.

1. Introduction

In a recent paper by Cooks et al. [1], the authors have summarized the importance of ion-molecule reactions measured in the gas phase at low gas densities, and many diverse applications of ion-molecule reactions to modern technologies were outlined. The importance of mass spectrometry studies to organic chemistry was emphasized. There is now a long list of named reaction mechanisms that have benefitted from sophisticated ion-molecule reaction studies. Pyridine and its derivatives are important in the chemical industry and ion-molecule reactions involving pyridine have received increased recent attention [2]. In an earlier paper we measured the electron impact ionization and ion-molecule reactions of pyridine [3], and found that $C_4H_4^+$ formed by electron impact on pyridine reacts with the parent molecule C_5H_5N via the reactions:

$$C_4H_4^+ + C_5H_5N \rightarrow C_5H_6N^+ + C_4H_3 \quad (34\%) \tag{1}$$

$$C_4H_4^+ + C_5H_5N \rightarrow C_5H_5N^+ + C_4H_4 \quad (12\%) \tag{2}$$

$$C_4H_4^+ + C_5H_5N \rightarrow C_9H_8N^+ + H \quad (54\%) \tag{3a}$$

where the branching ratios are shown in parentheses. $C_5H_5N^+$ in turn undergoes a secondary reaction with C_5H_5N to form $C_5H_6N^+$ [3]. Reactions (1) and (2) are proton transfer and charge transfer, respectively, while reaction (3a) is condensation with H-elimination. Reaction (3a) is of interest in terms of basic chemistry with regard to the structure of the product ion and the reaction mechanism. Earlier theoretical studies on adducts of selected ions with pyridine indicated that the reaction site of pyridine is the N atom [4–7]. However, in a recent study on the condensation reaction between pyridine with $C_5H_4N^+$ generated by electron impact ionization on pyridine, it was proposed that the reaction site is on the meta position of the pyridine [2]. In our previous study [3], we found that the H atom being eliminated in the condensation process can be from either the ionic reactant or pyridine, according to our experimental observation of the reaction of $C_4D_4^+$ with pyridine:

$$C_4D_4^+ + C_5H_5N \rightarrow C_9H_5D_3N^+ + D \tag{3b}$$

$$C_4D_4^+ + C_5H_5N \rightarrow C_9H_3D_4N^+ + H \tag{3c}$$

with a (3b) vs. (3c) branching ratio of ~2:1. The loss of the H atom from pyridine suggests that other reaction sites of pyridine besides the N atom are involved in the reaction mechanism.

To investigate the condensation-H-elimination reaction (3a), in the present study we perform theoretical calculations on possible structures of the product ions and experiments using Fourier transform mass spectrometry (FTMS) on gas-phase ion-molecule reactions of $C_4D_4^+$ with pyridine and substituted pyridines. Based on the results of the calculations and experiments, new insights are obtained and the condensation reaction pathway is discussed.

* Corresponding author. Tel.: +1 937 2552246; fax: +1 937 6564657.
E-mail address: alan.garscadden@wpafb.af.mil (A. Garscadden).

1387-3806/$ – see front matter. Published by Elsevier B.V.
doi:10.1016/j.ijms.2009.07.009

2. Experimental and theoretical methods

All of the experiments are performed using a modified FTMS equipped with a cubic ion cyclotron resonance (ICR) trapping cell (5 cm on a side) and a 2 T superconducting magnet [3,8]. The theory and methodology of FTMS have been well documented in the literature [9–11]. Pyridine-d_5 (C_5D_5N, 100.0 at.% D, Aldrich) and one of the pyridines (pyridine or substituted pyridines): pyridine (C_5H_5N, 99.9+%, Aldrich), 2,6-dimethylpyridine (2,6-$C_5H_3(CH_3)_2N$, 99+%, Sigma–Aldrich), 3,5-dimethylpyridine (3,5-$C_5H_3(CH_3)_2N$, 98+%, Aldrich), or 4-methylpyridine (4-$C_5H_4CH_3N$, 99%, Aldrich), are introduced into the FTMS system through two precision leak valves, respectively. The pressure ratio of pyridine-d_5 to pyridine or one of the substituted pyridines is set to approximately 1:1 using the ionization gauge, while total pressure of the mixture in the ICR cell is in the range of 10^{-7} Torr. For these measurements, an accurate pressure ratio is not required so the ionization gauge readout is adequate. The reactant ion $C_4D_4^+$ is generated along with other ions by electron impact ionization on C_5D_5N in the mixture. For the experiment where the reaction of $C_4H_4^+$ with C_5D_5N is studied, electron impact ionization on C_5H_5N produces the reactant ion. An electron gun (Kimball Physics ELG2, Wilton, NH) is used to irradiate the cell with a few hundred picocoulombs of 50-eV electrons to produce ionization. The motion of the ions is constrained radially by the superconducting magnetic field and axially by a 3-V electrostatic potential applied to the trap faces that are perpendicular to the magnetic field. $C_4D_4^+$ or $C_4H_4^+$ is selected from other ions generated by electron impact ionization of the gas mixture, using Stored Waveform Inverse Fourier Transform (SWIFT) [12–14] applied to two opposing trap faces which are parallel to the magnetic field. A time delay varying from 0 to 300 ms is inserted between the ion selection and ion detection to allow $C_4D_4^+$ or $C_4H_4^+$ to react with the gas mixture. For ion detection, ions of all mass-to-charge ratios are simultaneously and coherently excited into cyclotron orbits using SWIFT. Following the cyclotron excitation, the image currents induced on the two remaining faces of the trap are amplified, digitized and Fourier analyzed to yield a mass spectrum.

Quantum chemical calculations were performed to predict the structures and relative stabilities of multiple possible isomers and transition states of potential reaction intermediates $C_9H_8N^+$ and $C_9H_9N^+$. Specifically, second order perturbation theory methods (denoted as MP2, and also known as MBPT(2)) [15] were used in conjunction with the 6-311G(d,p) basis set [16], denoted as MP2/6-311G(d,p) for closed shell systems, whereas "Z-averaged" second order perturbation theory [17] (ZAPT(2)/6-311G(d,p)) was employed for open-shell species. Relative energies were refined using "completely renormalized" coupled cluster [18] single point energy calculations (denoted as CR-CCL(2,3)/6-311G(d,p)//MP2/6-311G(d,p) and CR-CCL(2,3)/6-311G(d,p)//ZAPT(2)/6-311G(d,p) for closed and open shell systems, respectively, or simply as CR-CCL for notational convenience). Local minima were verified as such by diagonalization of the matrix of energy second derivatives with respect to nuclear coordinates (i.e., the Hessian matrix). Zero-point vibrational energy corrections were obtained using harmonic frequencies scaled by a factor of 0.9748 [19]. All computations were performed using the GAMESS [20] quantum chemistry code.

3. Results and discussion

Because the nitrogen atom in pyridine possesses a pair of non-bonding electrons, reactions of cations with pyridine tend to proceed through the ion-dipole interaction between the ions and the nitrogen atom of pyridine. A recent theoretical study by Pullman et al. [4] on the reactions of tetramethylammonium ion (TMA^+) with aromatics has found that whereas benzene interacts with TMA^+ through the "cation-π" binding, the more polar molecule, pyridine, interacts more strongly with TMA^+ and adopts an orientation with its nitrogen atom toward the ion to maximize the N–N Coulomb attraction. In a study on reactions of SF_3^+ with benzene and pyridine by Sparrapan et al. using ab initio calculations [6], similar results are found: pyridine-SF_3^+ is covalently bonded through nitrogen while benzene-SF_3^+ is a loosely bonded π complex. Even the *ortho*-substituted pyridines can form N-coordinated binding with SiF^+ and SiF_3^+ [5], not hindered by the steric factor. In a theoretical study by Rodgers et al. [7] metal ions also prefer to bind to the nitrogen atom rather than to the π cloud of the aromatic ring of pyridine.

From the results of the above studies, the mechanism of the condensation reaction of $C_4H_4^+$ with pyridine may be envisioned as occurring via the formation of a covalent bond between N atom of pyridine and a C atom of $C_4H_4^+$, followed by loss of an H atom from the C_4H_4 moiety. However, this mechanism cannot explain the experimental observation that H atoms originally from either pyridine or $C_4H_4^+$ can be eliminated, as mentioned in the Introduction. Therefore, a modified N-coordinated reaction mechanism will be explored.

$C_4H_4^+$ is generated in our FTMS experiments by electron impact ionization of pyridine, and is believed to consist of two stable isomers, namely, vinylacetylene cation (VA^+) and methylene cyclopropene cation (MCP^+). In a study by Lifshitz et al. [21] on the gas-phase chemistry of $C_4H_4^+$, reactions between $C_4H_4^+$ and pyridine including proton transfer were observed, with the decay of $C_4H_4^+$ showing a single-exponential decay, but in the reactions of $C_4H_4^+$ with benzene, the decay of $C_4H_4^+$ was found to be double-exponential, which the authors considered as an indication of the presence of two $C_4H_4^+$ structures. In a study by Ausloos [22] on the structure of $C_4H_4^+$ produced by electron impact ionization of benzene and pyridine, it was claimed that at least two different $C_4H_4^+$ isomers were present, one which reacted with benzene and one which did not. Using ion-molecule reactions involving compounds with varying ionization energies (IEs) to bracket the IEs of the reactive and unreactive $C_4H_4^+$, the author identified these two forms of $C_4H_4^+$ as VA^+ and MCP^+, respectively, whose populations were 50:50 when formed by 15-eV electron impact on pyridine. In a study by Wagner-Redeker et al. [23] on the structure and reactivity of $C_4H_4^+$, two stable isomers were also identified by the authors, the linear isomer VA^+ and the cyclic isomer MCP^+, in agreement with observations of Ausloos. The linear isomer reacted with C_2H_2 at a rate constant of $3 \pm 1.5 \times 10^{-10}$ cm^3/s while the cyclic isomer reacted extremely slowly [23]. As mentioned in our previous paper [3], we observed no obviously double-exponential decay of $C_4H_4^+$ in its reaction with pyridine. This observation does not preclude the possibility of multiple isomers of $C_4H_4^+$. To probe this possibility, the experimental data of the $C_4H_4^+$ reaction are re-examined by fitting them to different kinetic models, shown in Fig. 1, where the symbols are the experimental data of the ion intensities acquired after a cooling period of 0.3 s (under $\sim 1 \times 10^{-5}$ Torr total pressure of Ar and pyridine) for $C_4H_4^+$ to be thermalized prior to the reaction [3]. The dashed lines are the fits of a kinetic model assuming only one isomer of $C_4H_4^+$, as described by equations (4)–(7):

$$C_4H_4^+ + C_5H_5N \rightarrow C_9H_8N^+ + H \quad (4)$$

$$C_4H_4^+ + C_5H_5N \rightarrow C_5H_5N^+ + C_4H_4 \quad (5)$$

$$C_4H_4^+ + C_5H_5N \rightarrow C_5H_6N^+ + C_4H_3 \quad (6)$$

$$C_5H_5N^+ + C_5H_5N \rightarrow C_5H_6N^+ + C_5H_4N \quad (7)$$

with the fitting parameters, the rate constants of reactions (4)–(7), as 5.9 ± 0.1, 0.3 ± 0.1, 2.7 ± 0.1 and 2.0 ± 1.4 s^{-1}, respectively. The solid lines are the fits of a kinetic model based on an assumption of

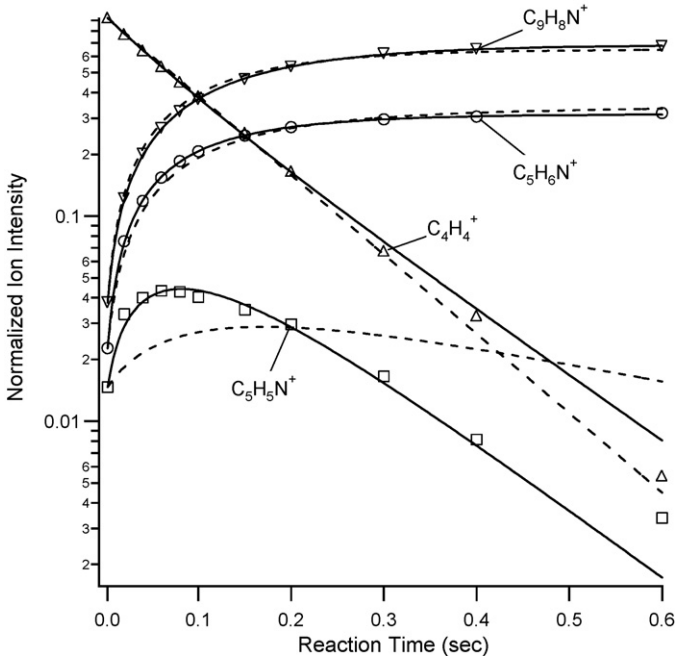

Fig. 1. Reaction time dependencies of ion intensities in the reaction of $C_4H_4^+$ with C_5H_5N. Symbols are experimental data, while the dashed lines are the fits of a kinetic model described by Eqs. (4)–(7), and solid lines are fits of a kinetic model described by Eqs. (8)–(12) (see the text).

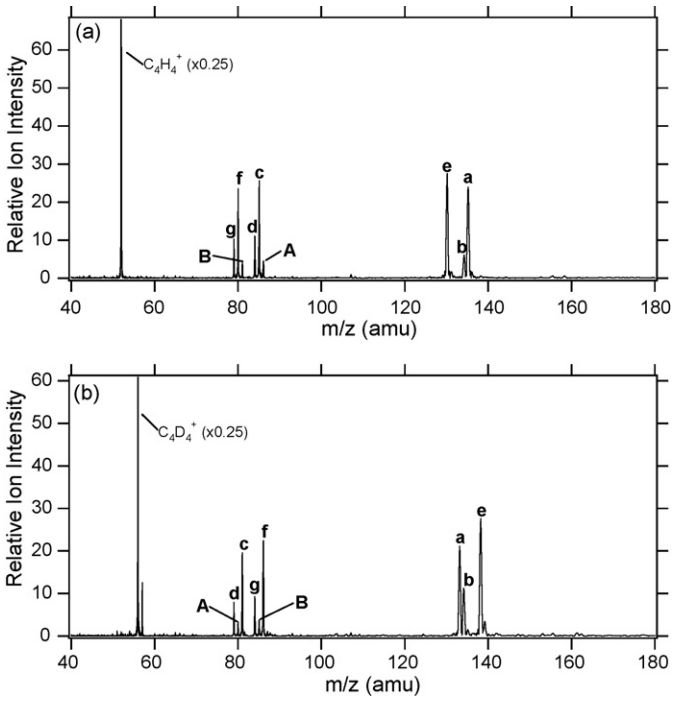

Fig. 2. Mass spectrum of reaction of (a) $C_4H_4^+$ and (b) $C_4D_4^+$ with a mixture of C_5H_5N/C_5D_5N in a ratio of ~1:1. The peak height of the reactant ion has been scaled by a factor of 1/4.

two $C_4H_4^+$ isomers, namely, MCP^+ and VA^+:

$$MCP^+ + C_5H_5N \rightarrow C_9H_8N^+ + H \quad (8)$$

$$VA^+ + C_5H_5N \rightarrow C_9H_8N^+ + H \quad (9)$$

$$VA^+ + C_5H_5N \rightarrow C_5H_5N^+ + C_4H_4 \quad (10)$$

$$VA^+ + C_5H_5N \rightarrow C_5H_6N^+ + C_4H_3 \quad (11)$$

$$C_5H_5N^+ + C_5H_5N \rightarrow C_5H_6N^+ + C_5H_4N \quad (12)$$

The resultant fitting parameters are 7.3 ± 0.2, 0.9 ± 0.9, 3.7 ± 0.4, 10.3 ± 0.7, $7.6 \pm 0.7\ s^{-1}$ for the rate constants of reactions (8)–(12), respectively, and $68 \pm 2\%$ for the percentage of MCP^+ in the $C_4H_4^+$ population before the reaction. From Fig. 1 it can be seen that while the one-isomer model fits the experimental data poorly, especially for $C_5H_5N^+$, the two-isomer model fits the data reasonably well except for the last data points of $C_5H_5N^+$ and $C_4H_4^+$ (these two data points may have large relative errors due to their low magnitudes). The kinetic model in (8)–(12) is based on the following thermochemical consideration: the IEs of C_5H_5N, MCP and VA are 9.25, 8.15, and 9.58 ± 0.02 eV [24], and the acidities of $C_5H_6N^+$, MCP^+ and VA^+ are 9.63 [25], 10.37 [26], and 8.53 eV [26], respectively, which indicate that VA^+ can undergo charge transfer and proton transfer with C_5H_5N ((10) and (11)) but MCP^+ cannot. We have considered another two-isomer kinetic model in which MCP^+ cannot undergo condensation (8) at all, but the fitting result is as poor as the one-isomer model in (4)–(7). Data fitting based on two energy states of $C_4H_4^+$, the ground state that has the condensation reaction channel and an excited state that has all reaction channels and can relax to the ground state, is very close to the fitting of the two-isomer model, and therefore the possibility of excited state ions being involved in the reactions cannot be excluded. Based on the discussions in the referenced papers [21–23] and the thermochemical data mentioned above, it appears that the two-isomer kinetic model in (8)–(12) describes the reaction of the majority of the $C_4H_4^+$ population. Since the reaction rate of (8) is a factor of 8 larger than that of (9), which means that the condensation is dominated by the reaction of MCP^+, in the rest of the paper we focus our discussion on MCP^+ in its condensation with pyridine.

Fig. 2a shows a typical reaction spectrum of $C_4H_4^+$ with a mixture of C_5H_5N/C_5D_5N (1:1) after a 20-ms reaction time and, for comparison, Fig. 2b shows a reaction spectrum of $C_4D_4^+$ with the mixture of C_5H_5N/C_5D_5N. The reaction time and the reactant gas pressures are chosen such that the mass spectrometer samples the ion population at an early reaction stage in which the primary product ions are unquestionably observed and yet the secondary reactions are not significant enough to severely complicate the ion population. Peaks in the spectra are labeled to indicate the reaction type rather than the product ion composition, e.g., 'a' indicates condensation with the loss of H (or D) atom originally from the ionic reactant, while 'b' indicates condensation with the loss of H (or D) atom originally from the neutral reactant; 'd' is the charge transfer between reactants that have different H-isotope content, while 'g' is the charge transfer between reactants that have the same H-isotope content, as shown in the following equations:

For Fig. 2a:

$$C_4H_4^+ + C_5D_5N \rightarrow C_9D_5H_3N^+(135) + H \quad (a)$$

$$C_4H_4^+ + C_5D_5N \rightarrow C_9D_4H_4N^+(134) + D \quad (b)$$

$$C_4H_4^+ + C_5D_5N \rightarrow C_5D_5HN^+(85) + C_4H_3 \quad (c)$$

$$C_4H_4^+ + C_5D_5N \rightarrow C_5D_5N^+(84) + C_4H_4 \quad (d)$$

$$C_4H_4^+ + C_5H_5N \rightarrow C_9H_8N^+(130) + H \quad (e)$$

$$C_4H_4^+ + C_5H_5N \rightarrow C_5H_6N^+(80) + C_4H_3 \quad (f)$$

$$C_4H_4^+ + C_5H_5N \rightarrow C_5H_5N^+(79) + C_4H_4 \quad (g)$$

For Fig. 2b:

$$C_4D_4^+ + C_5H_5N \rightarrow C_9H_5D_3N^+(133) + D \quad (a)$$

$$C_4D_4^+ + C_5H_5N \rightarrow C_9H_4D_4N^+(134) + H \quad (b)$$

$C_4D_4^+ + C_5H_5N \rightarrow C_5H_5DN^+(81) + C_4D_3$ (c)

$C_4D_4^+ + C_5H_5N \rightarrow C_5H_5N^+(79) + C_4D_4$ (d)

$C_4D_4^+ + C_5D_5N \rightarrow C_9D_8N^+(138) + D$ (e)

$C_4D_4^+ + C_5D_5N \rightarrow C_5D_6N^+(86) + C_4D_3$ (f)

$C_4D_4^+ + C_5D_5N \rightarrow C_5D_5N^+(84) + C_4D_4$ (g)

The numbers in parentheses are the nominal masses of the product ions. The observation of 'c' and 'f' confirms the proposed proton transfer mechanism; similarly the observation of 'd' and 'g' confirms the proposed charge transfer mechanism. The two ions labeled "A" and "B" in the mass spectra are identified as secondary reaction product ions. For example, in Fig. 2a they are $C_5D_6N^+$ (86) and $C_5H_5DN^+$ (81) respectively, which cannot be formed directly by $C_4H_4^+ + C_5H_5N$ or $C_4H_4^+ + C_5D_5N$ because the reaction cannot be stoichiometrically balanced. In the investigation of the reaction time dependence of the mass spectrum, we found that while the reactant ion exponentially decays as a function of the reaction time, all primary product ions keep increasing in intensity except $C_5H_5N^+$ and $C_5D_5N^+$. These two ions decay after reaching maxima at ~100 ms because they undergo proton transfer [3] with pyridine, producing $C_5H_6N^+$, $C_5HD_5N^+$, $C_5D_6N^+$ and $C_5H_5DN^+$ as the secondary product ions:

$C_5H_5N^+ + C_5H_5N \rightarrow C_5H_6N^+(80) + C_5H_4N$ (13a)

$C_5H_5N^+ + C_5D_5N \rightarrow C_5D_5HN^+(85) + C_5H_4N$ (13b)

$C_5D_5N^+ + C_5H_5N \rightarrow C_5H_5DN^+(81) + C_5D_4N$ (13c)

$C_5D_5N^+ + C_5D_5N \rightarrow C_5D_6N^+(86) + C_5D_4N$ (13d)

The branching ratio of 'a' vs. 'b' is ~4:1 in Fig. 2a and ~2:1 in Fig. 2b. From these values we conclude that the loss of an H atom originally from the reactant ion is favored over the loss of an H atom from pyridine and that there is a kinetic isotope effect. That is, the observed branching ratio of 'a/b' is the combination of the favoring factor (F) and the isotope effect (k^H/k^D, in which k^H and k^D are the rate constants of reactions involving H atom or D atom, respectively):

For Fig. 2a:

$$F \times \left(\frac{k^H}{k^D}\right) \approx 4;$$

For Fig. 2b:

$$F \times \left(\frac{k^D}{k^H}\right) \approx 2.$$

Solving the above equations for F and k^H/k^D yields the favoring factor $F \approx 2.8$ and the expected kinetic isotope effect $k^H/k^D \approx 1.4$.

The reaction path for the combined condensation plus H-elimination reaction therefore must be able to account for: (1) elimination of H atoms originally from pyridine or $C_4H_4^+$, (2) the preferred elimination of an H atom originally from $C_4H_4^+$, and (3) the observed isotope effect.

In order to identify the most stable $[C_9H_9N]^+$ and $[C_9H_8N]^+$ isomers, several possible structures were computed as functions of (i) the point of attachment of the incoming $C_4H_4^+$ moiety to pyridine and (ii) the location of the substituent on the ring (*ipso*, *meta*, *ortho*, or *para*). Fig. 3 shows the ZAPT(2)/6-311G(d,p) optimized structures and relative energies of 14 isomers of $[C_9H_9N]^+$. The six isomers in Fig. 3a correspond to structures that could be formed by a hypothetical two-step process involving (i) proton transfer from MCP$^+$ to pyridine, followed by (ii) addition of the remaining C_4H_3 neutral radical (denoted as R_a in Fig. 3a) to the just-formed $[C_5H_6N]^+$ cation. The five isomers in Fig. 3b correspond to $[C_9H_9N]^+$ adducts obtained from the formal addition of the MCP$^+$ radical cation (denoted as R_b) in which the point of attachment to pyridine is the methylene carbon atom. Similarly, the three isomers in Fig. 3c are derived from the addition of MCP$^+$ via the central carbon atom in the three-membered ring (denoted as R_c) to pyridine.

The most stable of the 14 isomers is 2-R_c, in which one of the *ortho* hydrogen atoms in pyridine has migrated to the nitrogen atom and the R_c ligand is attached at the available *ortho* position. Isomer 2-R_b, the most stable of the five isomers in Fig. 3b, has an *ortho* geometry similar to 2-R_c and is less stable by only 3.0 kcal/mol. Note that an additional conformer of 2-R_b, labeled 2-R_b', was located and found to be higher in energy than 2-R_b by 4.8 kcal/mol. The six R_a isomers in Fig. 3a are considerably higher in energy and are not discussed further.

Similarly, Fig. 4a and b summarize the MP2/6-311G(d,p) optimized structures and relative energies of nine isomers of the $[C_9H_8N]^+$ cation. Figs. 4a and 4b shows six and three isomers, respectively, resulting from the formal elimination of H^+ from the pyridine ring moiety in the $[C_9H_9N]^+$ isomers shown in Fig. 3a and b, respectively. The most stable $[C_9H_8N]^+$ isomer is the *ortho*-substituted vinylacetylene derivative, labeled A-R_c in Fig. 4c. Similarly, the most stable of the six isomers in Fig. 4a, B-R_a, has an *ortho* substituent, although the para-substituted isomer D-R_a is essentially isoenergetic. Furthermore, the *ortho*-substituted isomer A-R_b is the most stable of the three structures shown in Fig. 4b. Thus, there is a consistent thermodynamic preference for formation of *ortho*-substituted isomers of $[C_9H_8N]^+$. Twenty-two additional $[C_9H_8N]^+$ structures were also computed but are not shown. These include (a) 7 high-energy isomers formed by attachment of MCP$^+$ to pyridine via one of the carbon atoms in the cyclopropene ring, with energies ranging from 27 to 93 kcal/mol relative to A-R_c, and (b) 15 isomers derived from the less stable VA$^+$ and BT$^+$ isomers of $C_4H_4^+$.

The above theoretical results suggest that the *ortho* position of pyridine may be involved in the reaction mechanism. To verify this issue, we have performed experiments using pyridines substituted by methyl groups in *ortho*, meta and para positions, i.e. 2,6-$C_5H_3(CH_3)_2N$, 3,5-$C_5H_3(CH_3)_2N$ and 4-$C_5H_4CH_3N$, respectively, for the purpose of probing possible steric blocking. The steric blocking technique has been used in mass spectrometer studies to investigate ion fragmentation mechanisms [28–32]. For example, substitution of *ortho* positions of n-butylbenzene molecule by methyl groups has been found to suppress the hydrogen rearrangement completely. This is considered an indication that the rearrangement involves a six-membered transition state involving the side chain and the *ortho* position [28].

Fig. 5 shows the reaction mass spectrum of $C_4D_4^+$ with 2,6-$C_5H_3(CH_3)_2N$/C_5D_5N, 3,5-$C_5H_3(CH_3)_2N$/C_5D_5N and 4-$C_5H_4CH_3N$/C_5D_5N, respectively, with peaks identified as the product ions of the following reactions:

$C_4D_4^+ + 2,6\text{-}C_5H_3(CH_3)_2N \rightarrow C_{11}H_9D_3N^+(161) + D$ (a)

$C_4D_4^+ + 2,6\text{-}C_5H_3(CH_3)_2N \rightarrow C_{11}H_8D_4N^+(162) + H$ (b)

$C_4D_4^+ + 2,6\text{-}C_5H_3(CH_3)_2N \rightarrow C_7H_9DN^+(109) + C_4D_3$ (c)

$C_4D_4^+ + 2,6\text{-}C_5H_3(CH_3)_2N \rightarrow C_7H_9N^+(107) + C_4D_4$ (d)

$C_4D_4^+ + 3,5\text{-}C_5H_3(CH_3)_2N \rightarrow C_{11}H_9D_3N^+(161) + D$ (a)

$C_4D_4^+ + 3,5\text{-}C_5H_3(CH_3)_2N \rightarrow C_{11}H_8D_4N^+(162) + H$ (b)

$C_4D_4^+ + 3,5\text{-}C_5H_3(CH_3)_2N \rightarrow C_7H_9DN^+(109) + C_4D_3$ (c)

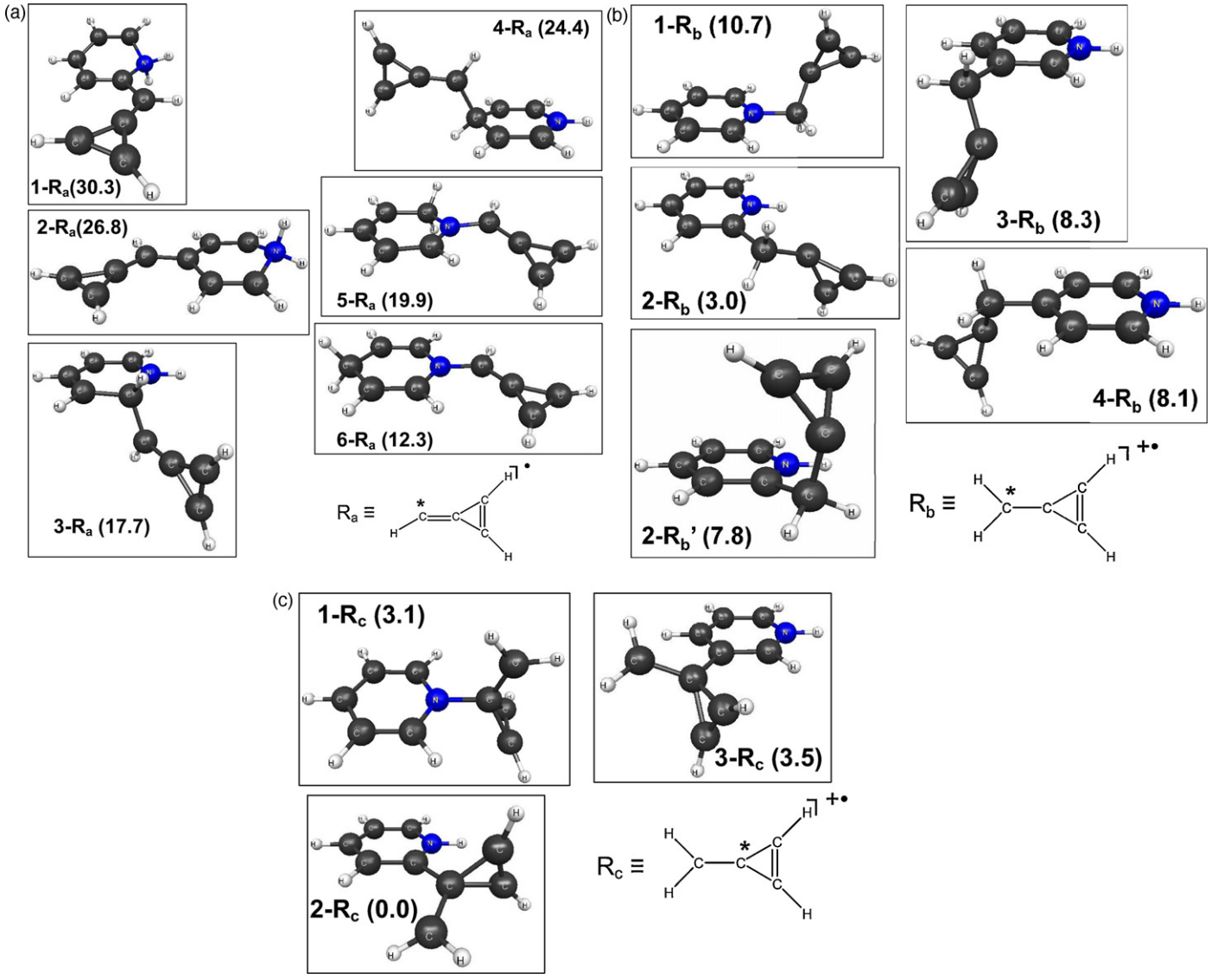

Fig. 3. ZAPT(2)/6-311G(d,p) structures and relative energies, enclosed in parentheses (in kcal/mol, including scaled zero-point vibrational energy corrections) of $C_9H_9N^+$ isomers. The carbon atom marked by an asterisk in the R_x fragment is the point of attachment to the pyridine ring.

$$C_4D_4^+ + 3,5\text{-}C_5H_3(CH_3)_2N \rightarrow C_7H_9N^+(107) + C_4D_4 \quad (d)$$

$$C_4D_4^+ + 4\text{-}C_5H_4(CH_3)N \rightarrow C_{10}H_7D_3N^+(147) + D \quad (a)$$

$$C_4D_4^+ + 4\text{-}C_5H_4(CH_3)N \rightarrow C_{10}H_6D_4N^+(148) + H \quad (b)$$

$$C_4D_4^+ + 4\text{-}C_5H_4(CH_3)N \rightarrow C_6H_7DN^+(95) + C_4D_3 \quad (c)$$

$$C_4D_4^+ + 4\text{-}C_5H_4(CH_3)N \rightarrow C_6H_7N^+(93) + C_4D_4 \quad (d)$$

and

$$C_4D_4^+ + C_5D_5N \rightarrow C_9D_8N^+(138) + D \quad (e)$$

$$C_4D_4^+ + C_5D_5N \rightarrow C_5D_6N^+(86) + C_4D_3 \quad (f)$$

$$C_4D_4^+ + C_5D_5N \rightarrow C_5D_5N^+(84) + C_4D_4 \quad (g)$$

As seen in Fig. 5a, in the reaction of $C_4D_4^+ + 2,6\text{-}C_5H_3(CH_3)_2N$, product ions 'a' and 'b' are significantly suppressed compared to Fig. 5b. In addition, a new product ion at m/z 148 marked by *, with a rather small branching ratio, is formed, probably due to a condensation-methyl-elimination:

$$C_4D_4^+ + 2,6\text{-}C_5H_3(CH_3)_2N \rightarrow C_{10}H_6D_4N^+(148) + CH_3$$

The above experimental results are in agreement with the assumption that the *ortho* positions of pyridine are involved in the condensation reaction. In comparison, 'a' and 'b' in Fig. 5b and c, for the reactions of $C_4D_4^+$ with 3,5-$C_5H_3(CH_3)_2N$ and 4-$C_5H_4CH_3N$ respectively, show no sign of reduced intensities compared to Fig. 2b, suggesting that the involvement of the meta and para positions of pyridine in the condensation reaction can be ruled out.

Based on the above discussion, a possible reaction pathway for (3) is as depicted in Scheme 1, which uses the methylene cyclopropene isomer as the structure for $C_4H_4^+$. The calculated atomic charges and spin populations of the species shown in the scheme are highly delocalized. Nonetheless, notional assignments of radical and charge sites are made in order to identify the key radical and charge migration steps in the proposed reaction pathways. As pointed out by Hoffmann and Stroobant [33], the radical and charge sites play important roles in deducing the reaction pathway; it is these sites that initiate certain electron movements within the ionized complex during rearrangement and cleavage processes, namely, radical migration and charge migration, respectively. In the scheme we denote the formal movement of individual electrons,

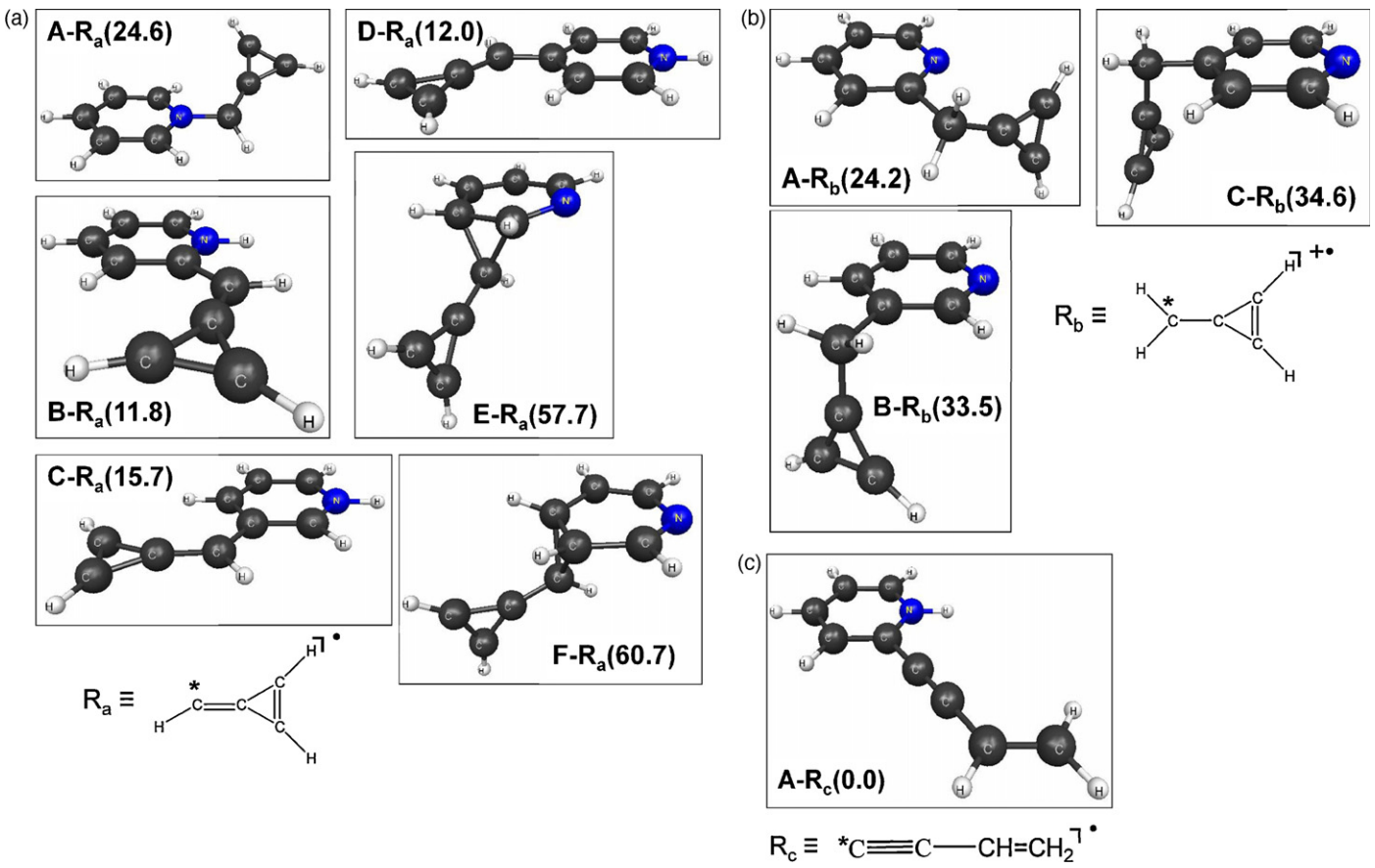

Fig. 4. MP2/6-311G(d,p) structures and relative energies, enclosed in parentheses (in kcal/mol, including scaled zero-point vibrational energy corrections) of $C_9H_8N^+$ isomers. The carbon atom marked by an asterisk in the R_x fragment is the point of attachment to the pyridine ring.

which results in radical migration, by the use of single-headed arrows.

The mechanism in Scheme 1 has been examined in detail using theoretical calculations. However, as illustrated in a recent study [27] of the $[C_5H_5N]^+ \rightarrow HCN + MCP^+$ reaction pathway, complete characterization of a reaction pathway can be quite challenging. Indeed, we do not claim that the pathway shown in Scheme 1 is the only possible mechanism which can account for the experimental observations noted above.

Fig. 6a illustrates the ZAPT(2)/6-311G(d,p) relative energies of several stationary points of a proposed mechanism for the $C_5H_5N + [C_4H_4]^+ \rightarrow [C_9H_9N]^+ \rightarrow C_9H_8N + H^+$ reaction channel. The corresponding CR-CCL(2,3)/6-311G(d,p)//ZAPT(2)/6-311G(d,p) relative energies, including scaled ZAPT(2)/6-311G(d,p) zero-point vibrational energy corrections, are shown in Fig. 6b and also are listed in Table 1. The stationary point geometries are illustrated in Fig. 7. The intermediates, each of which has all positive vibrational frequencies and therefore is a local minimum, are labeled I-*j* (*j* = 0–9) in Figs. 6 and 7 and Table 1. The transition states, each having exactly one imaginary frequency, are labeled as TS-*j*,*k* to denote that the minimum energy paths starting from TS-*j*,*k* lead to intermediates I-*j* and I-*k*. Note that transition states TS-2,2 and TS-4,4 connect energetically equivalent mirror images of intermediates I-2 and I-4, respectively. One of the stationary points shown in Fig. 6 has two imaginary frequencies and thus is a second order transition state, labeled as SOTS. With the exceptions of TS-2,3, TS-3,4, TS-4,4, and TS-4,6 (see below), the minimum energy paths connecting the transition states to the corresponding intermediates were traced using the second order Gonzales and Schlegel [34] or the linear (Euler) intrinsic reaction coordinate (IRC) algo-

Table 1
Predicted relative energies (in kcal/mol) of $[C_9H_9N]^+$ stationary points.

Geometry[a]	MP2[b]	MP2 + ZPE[b,c]	CR-CCL + ZPE[d]
Reactants	0.0	0.0	0.0
I-0 (C_s)	−15.9	−15.2	−13.2
I-1 (C_1)	−33.0	−29.2	−25.2
TS-1,2 (C_1)	−17.5	−16.9	−15.0
I-2 (C_1)	−38.6	−36.8	−32.1
TS-2,2 (C_s)	−33.9	−32.4	−27.5
TS-2,3 (C_s)	−11.1	−11.8	−5.6
TS-2,5 (C_1)	−7.1	−5.4	−3.5
I-3 (C_s)	−11.2	−8.7	−1.7
TS-3,4 (C_s)	−8.9	−9.2	−5.7
SOTS (C_s)	−16.9	−14.7	−12.2
I-4 (C_1)	−20.7	−18.0	−15.1
TS-4,4 (C_s)	−20.3	−17.6	−14.9
TS-4,6 (C_s)	22.6	21.3	28.3
I-5 (C_1)	−27.9	−21.5	−18.3
TS-5,6 (C_1)	45.1	42.9	51.0
TS-5,7 (C_1)	5.6	4.3	9.4
I-6 (C_s)	22.1	28.7	38.2
TS-6,7 (C_s)	28.2	26.4	32.2
I-7 (C_s) + H	−7.4	−10.3	0.3
TS-1,9 (C_1)	8.4	6.7	12.2
I-9 (C_1) + H	−0.5	−3.7	6.1
Products	−25.2	−28.3	−18.0

[a] Point group symmetry shown in parentheses.
[b] ZAPT(2)/6-311G(d,p)//ZAPT(2)/6-311G(d,p) energies, relative to $C_5H_5N + [C_4H_4]^+$ reactants.
[c] Including scaled ZAPT(2)/6-311G(d,p) zero-point vibrational energy corrections.
[d] CR-CCL(2,3)/6-311G(d,p)//ZAPT(2)/6-311G(d,p) energies, including scaled ZAPT(2)/6-311G(d,p) zero-point vibrational energy corrections, relative to $C_5H_5N + [C_4H_4]^+$ reactants.

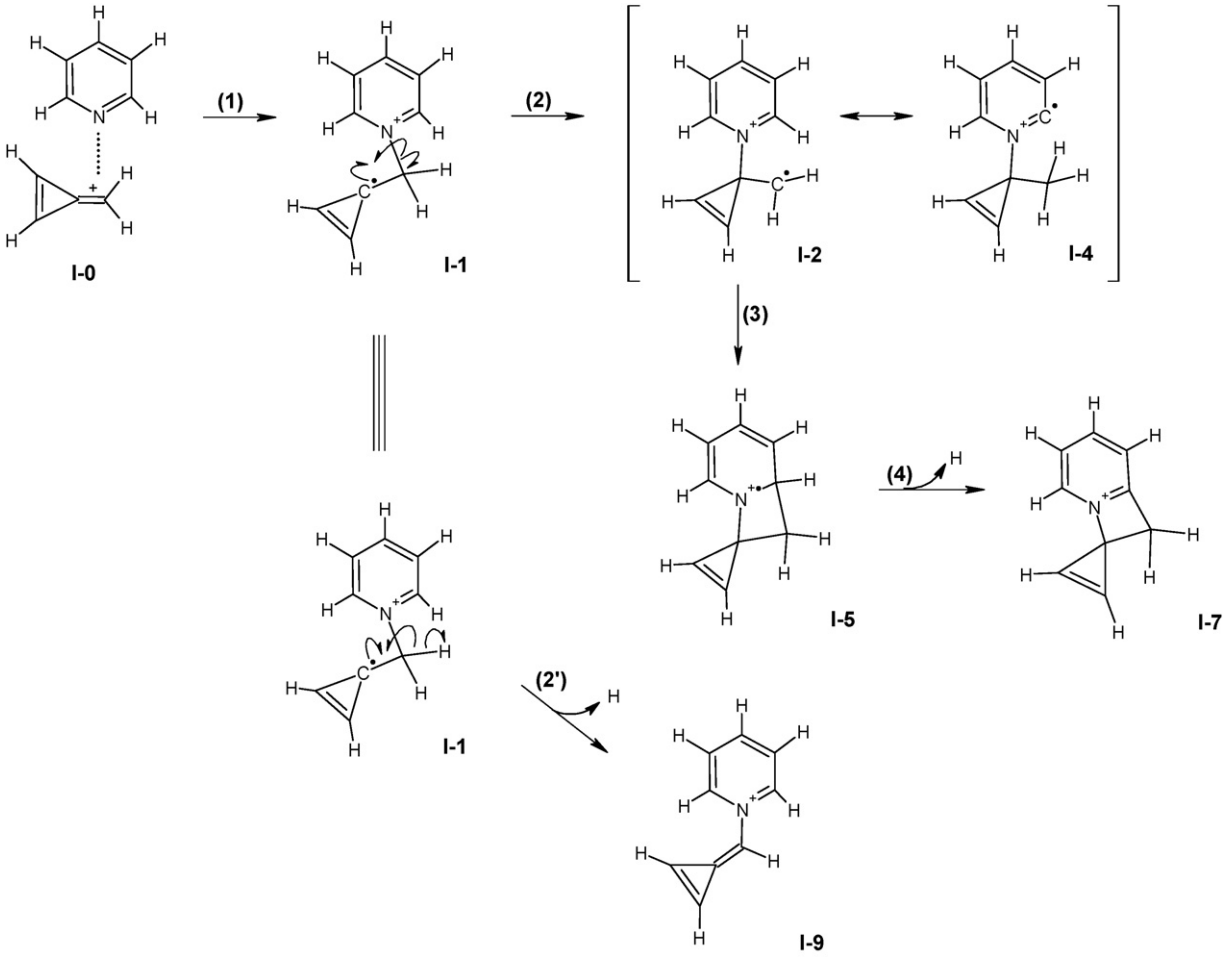

Scheme 1. A possible mechanism for the reaction of $C_4H_4^+$ + pyridine (see the text). The labels I-0, I-1, etc. correspond to those in Figs. 6 and 7.

rithms implemented in GAMESS. In the following discussion, all energies refer to the CR-CCL + ZPE level of theory unless otherwise noted.

The initial step of the proposed mechanism is the barrierless [35] formation of the ion-dipole complex "I-0" (shown in Fig. 7a) from the $C_5H_5N + [C_4H_4]^+$ reactants, which is downhill in energy by 13 kcal/mol. Also shown in Fig. 7a is a partial atomic numbering scheme labeling the key atoms in the proposed mechanism. The next step in the mechanism is the formation of a bond between the nitrogen atom and C_2, leading to intermediate I-1, shown in Fig. 7b. Several unsuccessful attempts were made to locate the intervening transition state TS-0,1. However, it appears that the barrier relative to I-0 is rather small as shown by a sequence of constrained geometry optimizations in which the R(N-C_2) distance was held fixed while the remaining geometrical degrees of freedom were fully optimized [36].

The next step in the mechanism is a carbon shift isomerization of I-1 via TS-1,2 (Fig. 7c) to form I-2 (Fig. 7d), in which the N-C_2 bond is broken and the N-C_3 bond is formed. (The additional reaction path from I-1 to form I-9 via TS-1,9 is discussed later.) This step has a barrier of about 10 kcal/mol relative to I-1 but the transition state is below the relative energy of the initial reactants by 15 kcal/mol. Isomer I-2 is the most stable of all the intermediates in the entire reaction scheme shown in Fig. 6, with an energy of −32 kcal/mol relative to the reactants. Two additional reaction pathways were found leading away from I-2, one of which forms I-3 (shown in Fig. 7f) via TS-2,3 (see Fig. 7e) and is the initial step of a hydrogen transfer from the β position in pyridine (C_1) to the C_2 atom in the original methylenecyclopropenium reactant. The remaining pathway from I-2, leading to formation of I-5 via TS-2,5, is discussed later.

There is a subtle point regarding the reaction pathway connecting I-2 and TS-2,3. Since the transition state TS-2,3 has C_s symmetry whereas the precursor I-2 has C_1 symmetry, the true minimum energy path connecting these stationary points necessarily passes through a bifurcation [37], at which point the symmetry of the minimum energy path changes from C_s to C_1. (Similar comments apply to the reaction path joining TS-3,4 and I-4 as well as the reaction pathway between TS-4,6 and I-4, which are discussed in more detail below.) The C_s symmetry-constrained pathway from TS-2,3 towards the precursor I-2, which diverges from the actual, C_1-symmetry minimum energy pathway beginning at the bifurcation, leads to another transition state TS-2,2, shown in Fig. 7g. The IRC starting from TS-2,2 proceeds smoothly to I-2, which suggests that the actual minimum energy pathway starting from TS-2,3 leads directly to I-2.Note that TS-2,3 and I-3 are nearly isoenergetic at the ZAPT(2)/6-311G(d,p) level, with I-3 only 0.1 kcal/mol lower in energy than TS-2,3, excluding ZPVE corrections. Inclusion of zero-point corrections actually reverses the order of relative stability, with TS-2,3 more stable than I-3 by 3.1 kcal/mol (see Table 1). The near degeneracy of these two stationary points is consistent with the remarkable similarity in the corresponding geometries, shown in Figs. 7e and 7f. The primary structural differences between these two stationary points are the R(C_1–H_1) and R(C_2–H_1) distances, which are 1.336 and 1.339, respectively, in TS-2,3, and 1.383 and 1.304, respectively, in I-3. In fact, the geometry of I-3, with a bridg-

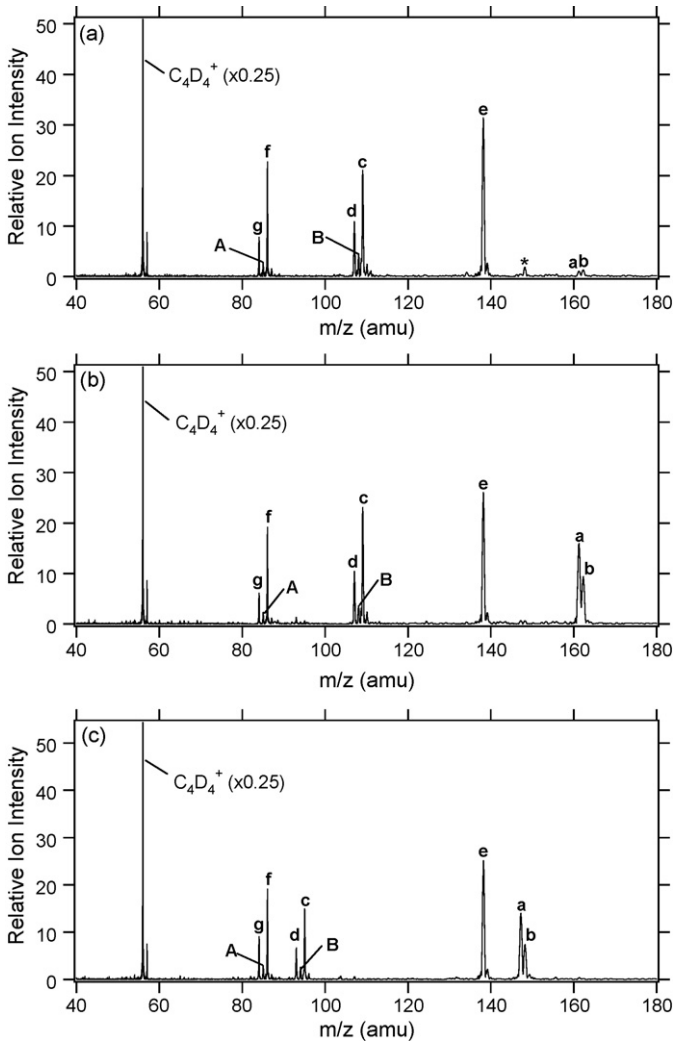

Fig. 5. Mass spectrum of reaction of $C_4D_4^+$ with a mixture of (a) 2,6-$C_5H_3(CH_3)_2N/C_5D_5N$, (b) 3,5-$C_5H_3(CH_3)_2N/C_5D_5N$ or (c) 4-$C_5H_4CH_3N/C_5D_5N$, in a ratio of ~1:1. The peak height of the reactant ion has been scaled by a factor of 1/4.

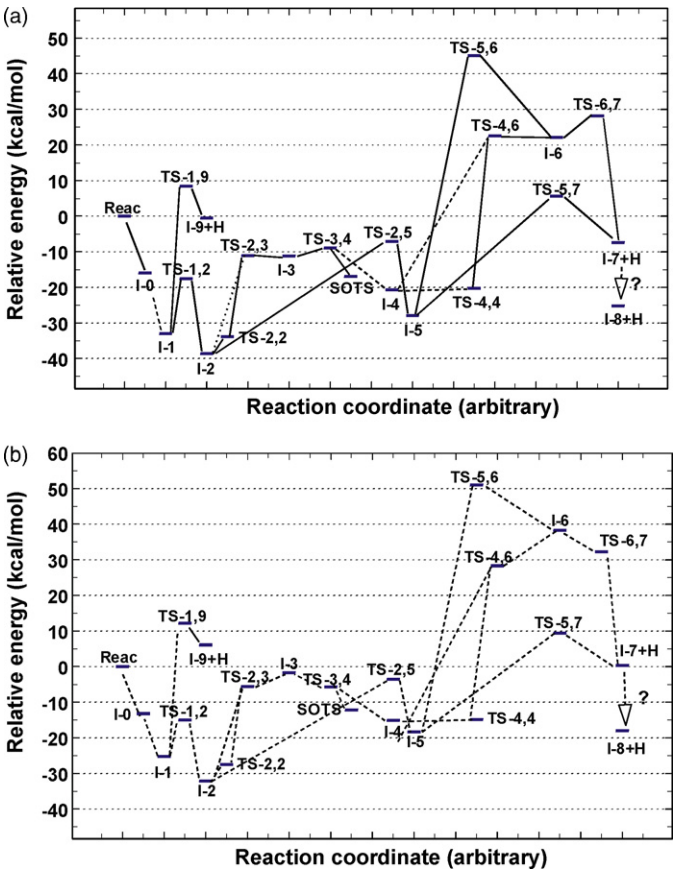

Fig. 6. Relative energies of reaction mechanism intermediates (I), transition states (TS), and second order transition states (SOTS). Solid lines denote reaction paths explicitly traced by intrinsic reaction coordinate (IRC) calculations. (a) ZAPT(2)/6-311G(d,p) relative energies. (b) CR-CCL(2,3)/6-311G(d,p)//ZAPT(2)/6-311G(d,p) relative energies, including ZAPT(2)/6-311G(d,p) scaled zero-point vibrational energy corrections.

ing C_1–H_1–C_2 linkage, is quite counterintuitive as a local minimum and may be an artifact of the ZAPT(2)/6-311G(d,p) theoretical level. This notion is consistent with the CR-CCL relative energies, which predict I-3 to be less stable than TS-2,3 by 3.9 kcal/mol and therefore suggest that I-3 may not be a true local minimum at higher level of theory (such as CR-CCL).

The next step in the H_1 transfer reaction is the formation of I-4 (see Fig. 7i) from I-3 via TS-3,4 (Fig. 7h), which has a barrier relative to I-3 of only 2.3 kcal/mol at the ZAPT(2)/6-311G(d,p) level. Inclusion of ZPVE reverses the order of relative stability of I-3 and TS-3,4, with the latter being more stable by 0.5 kcal/mol. Furthermore, at the CR-CCL level, TS-3,4 is more stable than I-3 by 4.0 kcal/mol. These results provide further evidence that I-3 may not be a local minimum at higher levels of theory.

As mentioned previously, there is a bifurcation along the reaction pathway connecting TS-3,4 and I-4. The C_s symmetry-constrained pathway from TS-3,4 leads to a second order transition state (SOTS, shown in Fig. 7j); i.e., a stationary point with two imaginary vibrational frequencies. Two geometry optimizations were subsequently performed, in which each optimization was initiated by stepping away from the SOTS along the transition vector corresponding to one of the imaginary frequencies. Both geometry optimizations readily converged to I-4, which suggests that the actual minimum energy pathway starting from TS-3,4 leads directly to I-4.

TS-4,4 (shown in Fig. 7k) is the transition state for internal rotation about the C_2–C_3–N–C_1 torsion angle. Although the small magnitude of the imaginary frequency (23i cm^{-1}) precluded tracing of the IRC, the minimum energy path presumably leads to I-4 [38]. The barrier relative to I-4 is only 0.2 kcal/mol, indicating that motion about the C_2–C_3–N–C_1 torsion angle is essentially unhindered.

Besides the hydrogen transfer reaction via TS-3,4 and the internal torsion via TS-4,4, the only other reaction pathway leading from I-4 is the initial stage in a combined C_1–C_2 ring closure plus hydrogen elimination process, to form I-6 (shown in Fig. 7m) via the C_s-symmetry transition state TS-4,6 (Fig. 7l). The barrier for this reaction relative to I-4 is approximately 43 kcal/mol and the transition state TS-4,6 lies 28 kcal/mol above the initial reactants. As mentioned previously, the actual minimum energy pathway joining TS-4,6 and I-4 goes through a bifurcation, at which point the symmetry of the reaction path changes from C_s to C_1. Tracing the C_s symmetry-constrained reaction path from TS-4,6 in the reverse direction of the transition vector shown in Fig. 7l leads to TS-4,4, which in turn leads to I-4. This suggests that the actual minimum energy path from TS-4,6 leads directly to I-4. Tracing the minimum energy path from TS-4,6 in the direction of the transition vector shown in Fig. 7l leads to I-6 (Fig. 7m). Similar to the case of I-3, the structure of I-6 is counterintuitive as a local minimum; i.e., the C_2 atom appears to be quasi-pentacoordinated, with unusually long bond lengths of 1.335 for C_2–H_{2b} and 1.832 angstroms

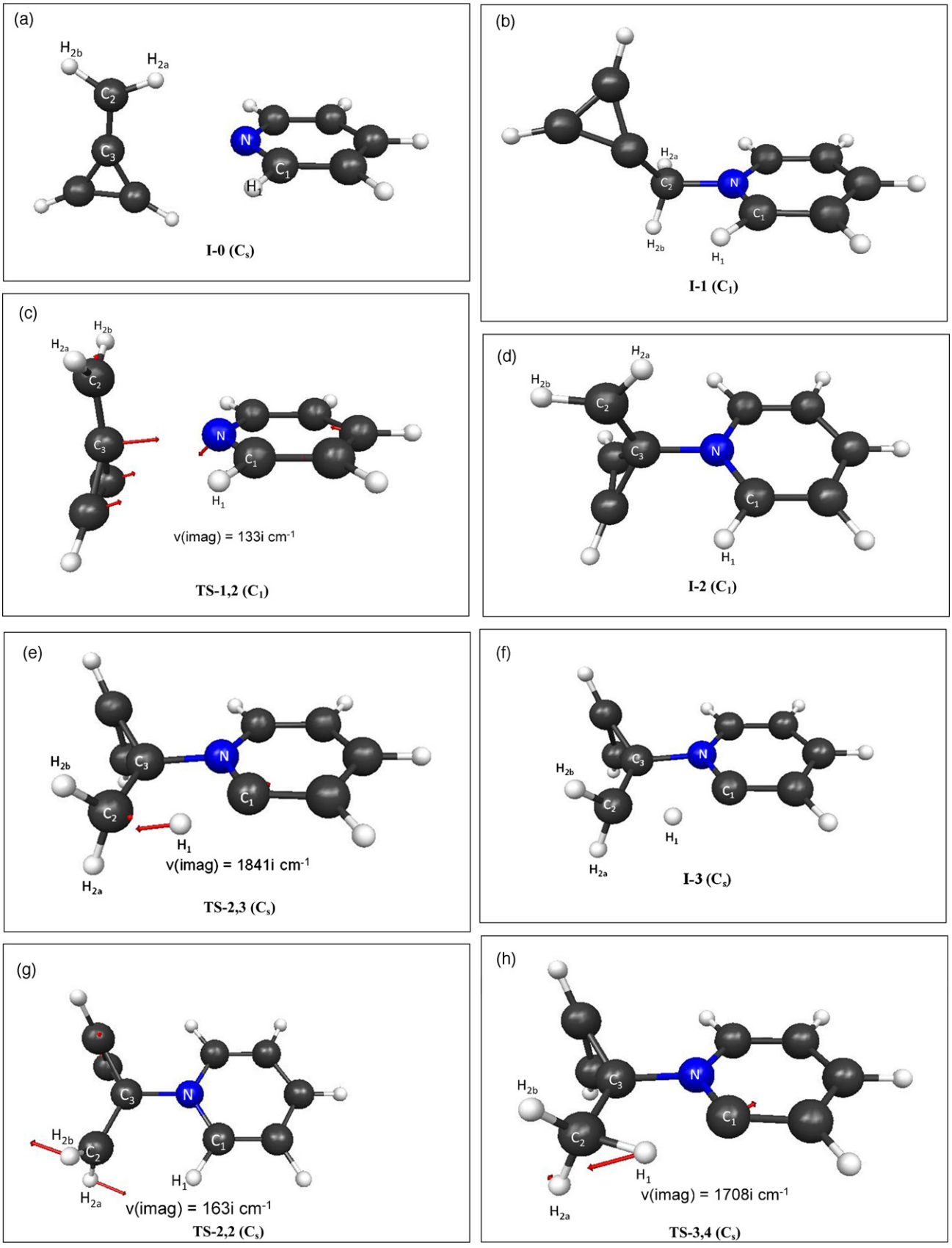

Fig. 7. ZAPT(2)/6-311G(d,p) structures of reaction mechanism intermediates (I), transition states (TS), and second order transition states (SOTS).

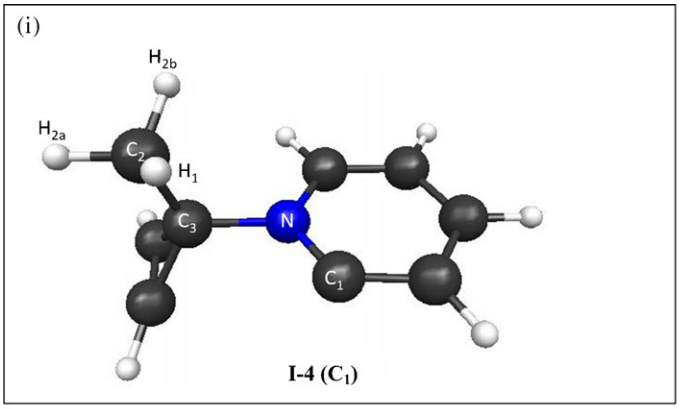

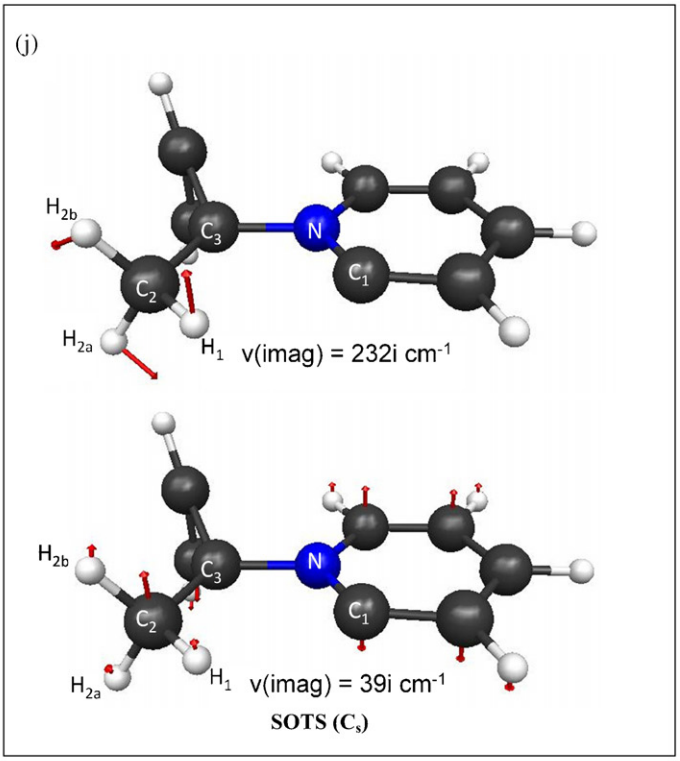

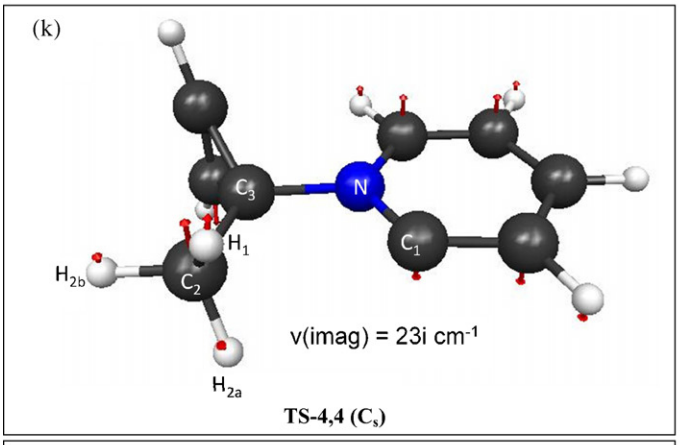

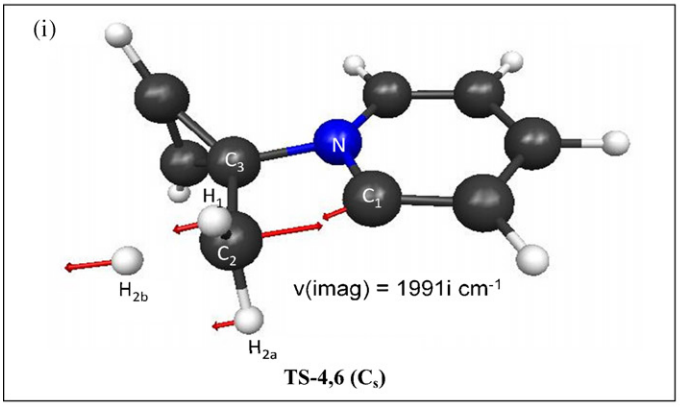

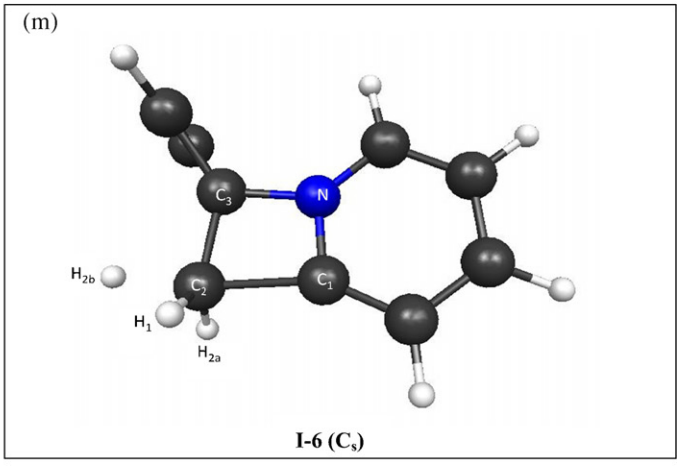

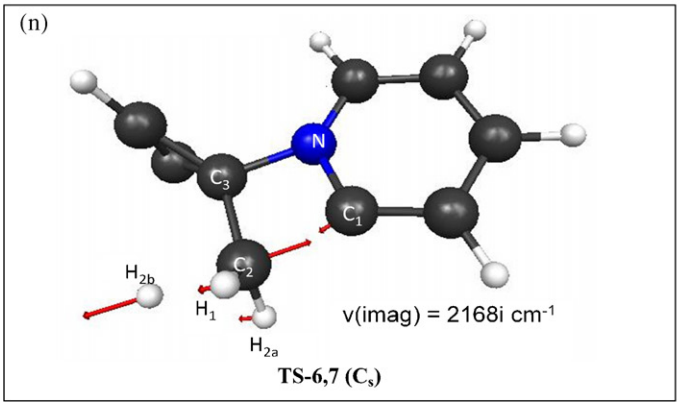

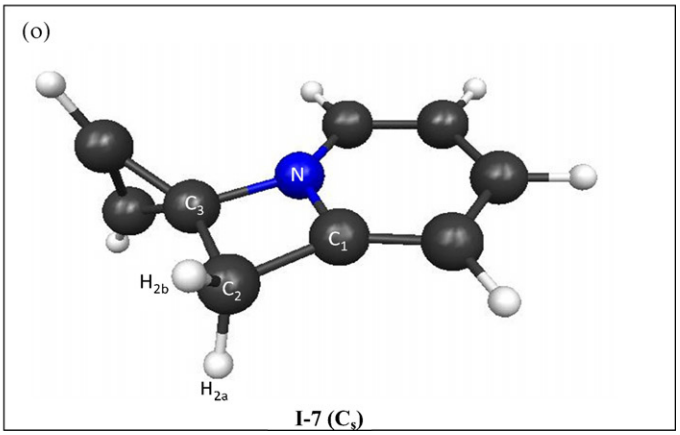

Fig. 7. (*Continued*)

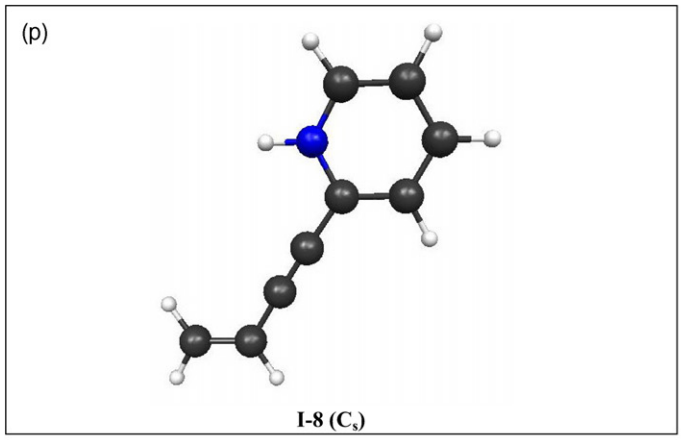

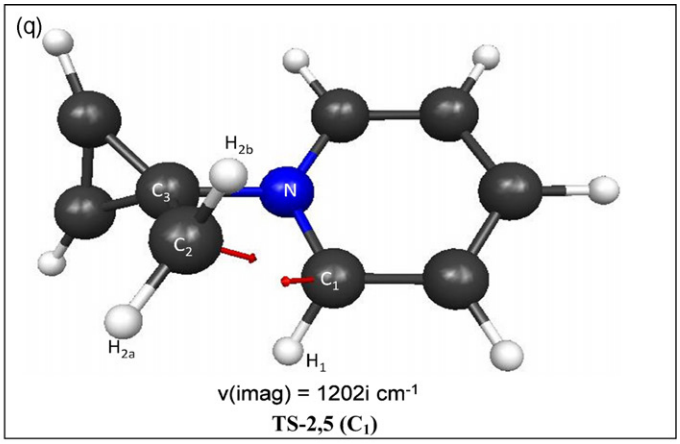

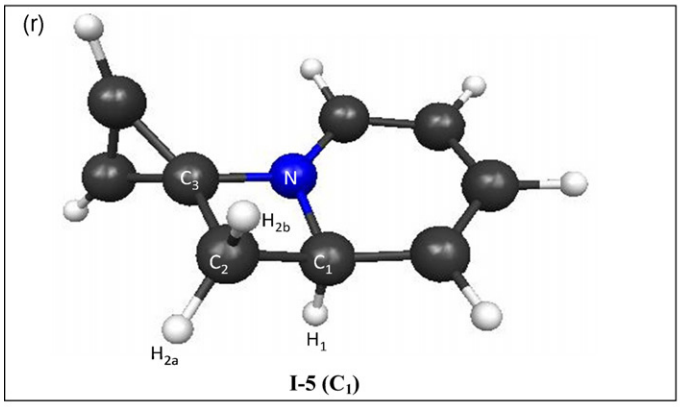

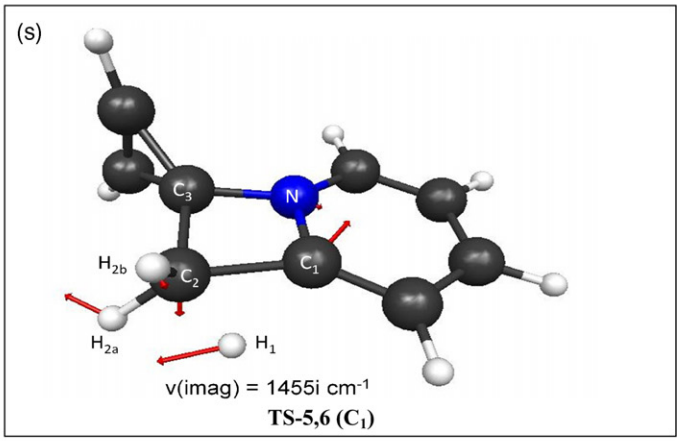

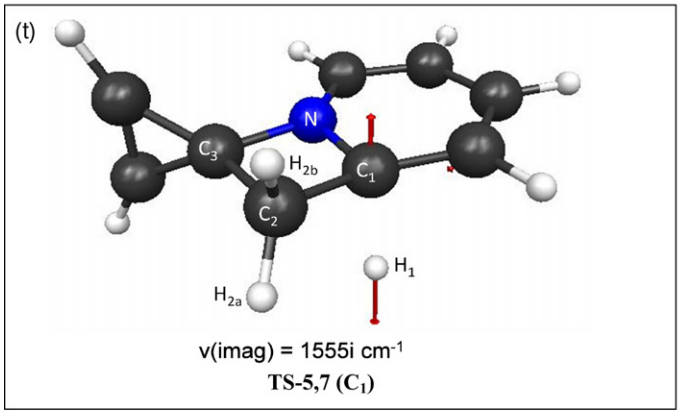

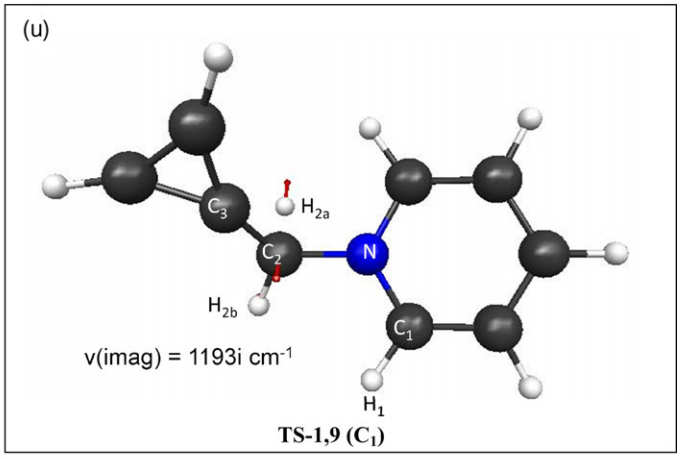

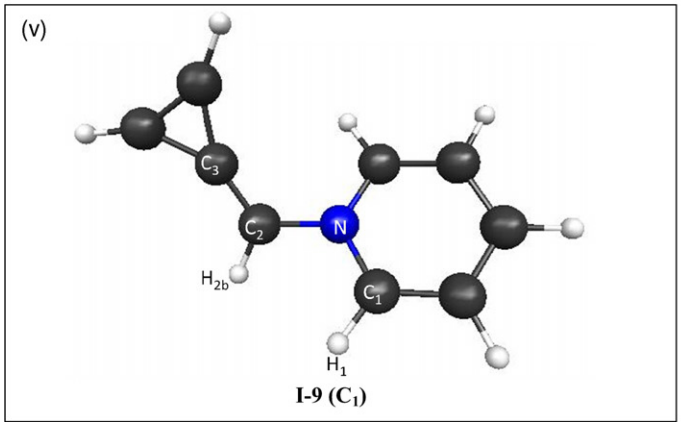

Fig. 7. (*Continued*).

for C_1–C_2. I-6 is only 0.5 kcal/mol more stable than TS-4,6 at the ZAPT(2)/6-311G(d,p) level, excluding ZPE corrections. Inclusion of ZPE effects reverses the order of relative stability, with TS-4,6 more stable than I-6 by 7.4 kcal/mol. Similarly, at the CR-CCL level TS-4,6 is more stable than I-6 by nearly 10 kcal/mol, thereby suggesting that I-6 may not be a local minimum at higher levels of theory.

TS-6,7, the transition state for the second stage of the C_1–C_2 ring closure plus H-elimination process, is shown in Fig. 7n and has an energy of 32 kcal/mol relative to the initial reactants. At the ZAPT(2)/6-311G(d,p) level, the barrier relative to I-6 is 6.1 kcal/mol, excluding zero-point vibrational energy corrections. Inclusion of the latter reverses the order of relative stability, with I-6 2.3 kcal/mol above TS-6,7. At the CR-CCL level, I-6 is higher in energy than TS-6,7 by 6.0 kcal/mol, which again suggests that I-6 may not be a local minimum at a more accurate level of theory. The products of this reaction step, I-7 (shown in Fig. 7o) + H, are only 0.3 kcal/mol above the initial reactants. Subsequent isomerization of I-7 to a more stable $C_9H_8N^+$ species such as I-8 (which is shown in Fig. 7p and is identical to A-R_c in Fig. 4c) is possible, although the mechanism of such a process is not considered further in the present study.

We now return to the third reaction pathway leading away from I-2; namely, the formation of I-5 (see Fig. 7r) via transition state TS-2,5 (Fig. 7q). This is a ring closure reaction, forming a C_1–C_2 bond. The barrier relative to I-2 is nearly 29 kcal/mol; TS-2,5 is nonetheless lower in energy than the initial reactants and therefore thermally accessible. There are two additional pathways leading from I-5, one of which is a hydrogen transfer from C_1 to C_2, leading to formation of I-6 via the saddle point TS-5,6, shown in Fig. 7s. The barrier relative to I-5 is 69 kcal/mol and the transition state is 51 kcal/mol higher in energy than the initial reactants. Therefore, this pathway is thermally inaccessible. The remaining reaction channel from I-5 is hydrogen elimination from C_1, leading to formation of I-7 (Fig. 7o) plus a hydrogen atom via saddle point TS-5,7 (Fig. 7t). The forward barrier for this step is 28 kcal/mol and TS-5,7 is 9.4 kcal/mol above the initial reactants.

Finally, we consider the second reaction channel from I-1; namely, the hydrogen elimination step to form I-9 (Fig. 7v) plus hydrogen via transition state TS-1,9 (Fig. 7u). Although the barrier for this reaction is 37 kcal/mol relative to I-1, the transition state is only 12 kcal/mol higher than the initial reactants and is comparable to the relative energy of TS-5,7 (9.4 kcal/mol).

These results explain four key experimental observations: (a) the presence of a kinetic isotope effect, (b) elimination of hydrogen from both the initial ionic ($C_4H_4^+$) and neutral (C_5H_5N) reactants, (c) the preferred elimination of hydrogen from $C_4H_4^+$, and (d) the steric blocking effect of methyl group substitution in the *ortho* positions of pyridine. First, we make a simplifying assumption. As illustrated in Fig. 6, formation of intermediate I-7 can occur via three pathways. Two of these pathways, namely I-5 → TS-5,6 → I-6 → TS-6,7 → I-7 + H and I-4 → TS-4,6 → I-6 → TS-6,7 → I-7 + H, must surmount substantially larger energy barriers than the third channel, I-5 → TS-5,7 → I-7 + H. Therefore, it is plausible that the formation of I-7 is dominated by the last route, with the former two channels playing only a minor role. With regard to energetics, the hydrogen elimination reaction channels I-5 → TS-5,7 → I-7 + H and I-1 → TS-1,9 → I-9 + H, which have similar barriers, are rate-limiting steps for the overall condensation reaction. Since these reaction steps correspond to elimination of an H or D atom, this sequence accounts for the observed kinetic isotope effect.

To examine the sequence in further detail, the effects of isotopic substitution on the energetics of the I-5 → TS-5,7 → I-7 and I-1 → TS-1,9 → I-9 + H reaction steps were computed at the CR-CCL level and are summarized in Table 2. For the reactants $C_4H_4^+ + C_5D_5N$, the forward barrier for elimination of an H atom via TS-5.7 is 27.7 kcal/mol, whereas for D atom elimination the barrier rises to 28.9 kcal/mol. Similarly, for the reactants $C_4D_4^+ + C_5H_5N$, the forward barrier via TS-5,7 is 27.8 kcal/mol for hydrogen elimination and 29.6 kcal/mol for elimination of a deuterium. Similar isotope effects are seen for the I-1 TS-1,9 → I-9 + H reaction. For the reactants $C_4H_4^+ + C_5D_5N$, the forward barrier for elimination of an H atom via TS-1,9 is 37.4 kcal/mol, whereas for D atom elimination the barrier rises to 39.0 kcal/mol. Likewise, the forward barrier via TS-1,9 for reactants $C_4D_4^+ + C_5H_5N$ is 37.5 kcal/mol for H atom elimination, but increases to 39.0 for elimination of a deuterium. In all cases, elimination of a D atom is energetically less favorable than H, which is consistent with the experimentally observed isotope effect.

Elimination of hydrogen atoms from both the cation and neutral reactants is explained by the pathways connecting I-2 and I-4. The net result of the sequence of steps connecting I-2 and I-4 is a H atom transfer between the C_1 atom in pyridine and the C_2 atom in the original $C_4H_4^+$ reactant. Once intermediate I-4 is formed, it is energetically more favorable to revert back to I-2 than to isomerize to I-6 via TS-4,6. Therefore, multiple interconversions between I-2 and I-4 can occur, causing a scrambling of the H_{2a} and H_{2b} hydrogen atoms originally from the $C_4H_4^+$ reactant with the two *ortho* hydrogens in pyridine. (It is reasonable to assume that internal rotation of the C_2 methyl group in I-4 is essentially unhindered, thereby facilitating the H atom scrambling.) In competition with the I-2 → I-4 reaction channel is the I-2 → I-5 pathway, which ultimately leads to the final products via I-7. Note that the barrier to form I-5 via

Table 2
Effects of isotopic substitution on the I-5 → TS-5,7 → I-7 + H and I-1 → TS-1,9 → I-9 + H reaction energetics.[a].

Geometry[a]	CR-CCL + ZPE[b]				
	$C_4H_4^+ + C_5H_5N$	$C_4H_4^+ + C_5D_5N$		$C_4D_4^+ + C_5H_5N$	$C_4D_4^+ + C_5D_5N$
	0.0[c]	0.0[c]		0.0[c]	0.0[c]
I-5	−18.3	−18.4[d]	−18.4[e]	−18.8[d]	−18.8[e]	−18.8
TS-5,7	9.4	9.3[d]	10.5[e]	9.0[d]	10.8[e]	10.4
I-7 + H/D	0.3	0.2[d]	2.4[e]	−0.1[d]	1.9[e]	1.9
I-1	−25.2	−25.3[d]	−25.3[e]	−25.6[d]	−25.6[e]	−25.8
TS-1,9	12.2	12.1[d]	13.7[e]	11.9[d]	13.4[e]	13.3
I-9 + H/D	6.1	6.0[d]	8.0[e]	5.7[d]	7.8[e]	7.7

[a] See Fig. 7 for structures of I-5, TS-5,7, I-7, I-1, TS-1,9, and I-9.
[b] CR-CCL(2,3)/6-311G(d,p)//ZAPT(2)/6-311G(d,p) energies, including scaled ZAPT(2)/6-311G(d,p) zero-point vibrational energy corrections, relative to $[C_4X_4]^+ + C_5Y_5N$ (X,Y = H or D).
[c] Reactants.
[d] H atom elimination.
[e] D atom elimination.

TS-2,5 is slightly higher than the barrier to formation of I-4 via TS-3,4 (28.6 and 26.4 kcal/mol, respectively, at the CR-CCL level), suggesting that H atom scrambling via I-2 ↔ I-4 interconversion may precede the I-2 → I-5 step.

Preferential elimination of hydrogen originally bound to the $C_4H_4^+$ reactant can be qualitatively explained in part by the I-1 → TS-1,9 → I-9 + H reaction step. Although H-atom scrambling via I-2 ↔ I-4 interconversion prior to the I-1 → TS-1,9 → I-9 + H reaction step is not precluded, it is nonetheless possible for the latter process to take place before scrambling occurs. Furthermore, in the absence of scrambling, the eliminated hydrogen atom necessarily is originally attached to $C_4H_4^+$. This qualitatively accounts for the observed preferential elimination of hydrogen from C4H4 + , to the extent that the I-1 → TS-1,9 → I-9 + H reaction step takes place prior to H-atom scrambling.

Therefore the global mechanism, illustrated in Scheme 1, can be viewed as consisting of four fundamental components: (1) formation of I-1, (2) competing steps of H atom elimination from I-1 (to form I-9 + H) and isomerization of I-1 to form I-2, (3) competing steps of H atom scrambling via I-2 ↔ I-4 interconversion and isomerization of I-2 to form I-5, and (4) elimination of a hydrogen atom from I-5 to form I-7.

Finally, the steric blocking effect of methyl substitution at the *ortho* position of pyridine is clear from the primary role of the *ortho* pyridine carbon in the mechanism illustrated in Scheme 1. Specifically, the presence of methyl groups in the *ortho* positions on pyridine would likely inhibit the formation of I-1 as well as preclude the subsequent formation of I-5 from I-2. Therefore, we interpret the observed reduced intensities of the condensation product ions in Fig. 5a for the reaction of $C_4D_4^+$ + 2,6-$C_5H_3(CH_3)_2N$ to be the result of this steric blocking effect, which occurs at the first step: the presence of the methyl group in the *ortho* positions of pyridine hinders the formation of the new N–C_2 σ bond in I-1. It is interesting to compare this reaction to the reaction of SiF^+ (or SiF_3^+) with 2,6-dimethylpyridine studied by Wang et al. [5], which, with the interaction occurring only at the N atom site, is not hindered but enhanced by the presence of the methyl groups at the *ortho* positions.

4. Summary

By means of theoretical calculations and experiments using deuterated pyridine and substituted pyridines, the reaction of $C_4H_4^+$ with pyridine (C_5H_5N) is investigated. A possible reaction scheme is proposed for the formation of a condensation-H-elimination product ion, $C_9H_8N^+$, from pyridine and the isomer MCP^+ of $C_4H_4^+$. In the scheme the initially formed ion-molecule complex undergoes a multi-step condensation consisting of (a) the formation of a σ bond between the nitrogen atom in pyridine and the terminal methylene group on MCP^+, followed by a carbon shift in which the newly formed C–N σ bond is broken and the nitrogen atom becomes bound to the central ring carbon in MCP^+, (b) establishment of a quasi-equilibrium involving H-atom migration between the *ortho* position in pyridine and the terminal methylene group in the MCP^+ moiety, (c) a ring closure step in which a C–C σ bond is formed between the terminal methylene group in MCP^+ and an *ortho* carbon in pyridine, and (d) elimination of a H atom to form the final $C_9H_8N^+$ product ion. This reaction scheme is consistent with the experimentally observed preference of loss of H atom originally from the reactant ion, the measured kinetic isotope effect, and the presumed steric blocking effect of methyl groups in the *ortho* positions of pyridine. We should point out that because the reaction system is a complex polyatomic one, there may be many other pathways for the H-elimination, and therefore the proposed reaction scheme is not necessarily an exclusive one.

Acknowledgements

The authors thank the Air Force Office of Scientific Research for support. Grants of computer time from the Department of Defense High Performance Computing Modernization Program at the Air Force Research Laboratory Wright-Patterson Air Force Base, OH, and the Engineer Research and Development Center, Vicksburg, MS, DoD Supercomputing Resource Centers are gratefully acknowledged.

We also thank a referee for a careful reading of the paper and valuable comments that enabled improvement of the paper.

Appendix A. Supplementary data

Supplementary data associated with this article can be found, in the online version, at doi:10.1016/j.ijms.2009.07.009.

References

[1] R.G. Cooks, H. Chen, M.N. Eberlin, X. Zheng, W.A. Tao, Chem. Rev. 106 (2006) 188.
[2] S. Yao, X. Zhang, L. Zhang, C. Wang, Y. Guo, Rapid Commun. Mass Spectrom. 21 (2007) 1739.
[3] C.Q. Jiao, C.A. DeJoseph Jr., R. Lee, A. Garscadden, Int. J. Mass Spectrom. 257 (2006) 34.
[4] A. Pullman, G. Berthier, R. Savinelli, J. Comput. Chem. 18 (1997) 2012.
[5] F. Wang, S. Ma, P. Wong, R.G. Cooks, F.C. Gozzo, M.N. Eberlin, Int. J. Mass Spectrom. 179/180 (1998) 195.
[6] R. Sparrapan, M.A. Mendes, M.N. Eberlin, Int. J. Mass Spectrom. 182/183 (1999) 369.
[7] M.T. Rodgers, J.R. Stanley, R. Amunugama, J. Am. Chem. Soc. 122 (2000) 10969.
[8] P.D. Haaland, Chem. Phys. Lett. 170 (1990) 146.
[9] M.B. Comisarow, A.G. Marshall, Chem. Phys. Lett. 25 (1974) 282.
[10] A.G. Marshall, P.B. Grosshans, Anal. Chem. 63 (1991) 215A.
[11] Z. Liang, A.G. Marshall, Anal. Chem. 62 (1990) 70.
[12] A.G. Marshall, T.L. Wang, T.L. Ricca, J. Am. Chem. Soc. 107 (1985) 7983.
[13] S. Guan, J. Chem. Phys. 91 (1989) 775.
[14] L. Chen, A.G. Marshall, Int. J. Mass Spectrom. Ion Processes 79 (1987) 115.
[15] (a) C. Møller, M.S. Plesset, Phys. Rev. 46 (1934) 618;
(b) J.A. Pople, J.S. Binkley, R. Seeger, Int. J. Quan. Chem. S10 (1976) 1;
(c) M.J. Frisch, M. Head-Gordon, J.A. Pople, Chem. Phys. Lett. 166 (1990) 275;
(d) R.J. Bartlett, D.M. Silver, Int. J. Quant. Chem. S9 (1975) 183;
(e) C.M. Aikens, S.P. Webb, R. Bell, G.D. Fletcher, M.W. Schmidt, M.S. Gordon, Theor. Chem. Acc. 110 (2003) 233.
[16] R. Krishnan, J.S. Binkley, R. Seeger, J.A. Pople, J. Chem. Phys. 72 (1980) 650.
[17] (a) T.J. Lee, D. Jayatilaka, Chem. Phys. Lett. 201 (1993) 1;
(b) T.J. Lee, A.P. Rendell, K.G. Dyall, D. Jayatilaka, J. Chem. Phys. 100 (1994) 7400;
(c) I.M.B. Nielsen, E.T. Seidl, J. Comput. Chem. 16 (1995) 1301;
(d) G.D. Fletcher, M.S. Gordon, R.L. Bell, Theor. Chem. Acc. 107 (2002) 57;
(e) C.M. Aikens, G.D. Fletcher, M.W. Schmidt, M.S. Gordon, J. Chem. Phys. 124 (2006) 014107/1.
[18] (a) P. Piecuch, M. Wloch, J. Chem. Phys. 123 (2005) 224105;
(b) M. Wloch, J.R. Gour, P. Piecuch, J. Phys. Chem. A 111 (2007) 11359.
[19] A.P. Scott, L. Radom, J. Phys. Chem. 100 (1996) 16502.
[20] (a) M.S. Gordon, M.W. Schmidt, in: C.E. Dykstra, G. Frenking, K.S. Kim, G.E. Scuseria (Eds.), Theory and Applications of Computational Chemistry, the first forty years, Elsevier, Amsterdam, 2005;
(b) M.W. Schmidt, K.K. Baldridge, J.A. Boatz, S.T. Elbert, M.S. Gordon, J.H. Jensen, S. Koseki, N. Matsunaga, K.A. Nguyen, S.J. Su, T.L. Windus, M. Dupuis, J.A. Montgomery, J. Comput. Chem. 14 (1993) 1347.
[21] C. Lifshitz, D. Gibson, K. Levsen, I. Dotan, Int. J. Mass Spectrom. Ion Phys. 40 (1981) 157.
[22] P. Ausloos, J. Am. Chem. Soc. 103 (1981) 3931.
[23] W. Wagner-Redeker, A.J. Illies, P.R. Kemper, M.T. Bowers, J. Am. Chem. Soc. 105 (1983) 5719.
[24] S.G. Lias, J.E. Bartmess, J.F. Liebman, J.L. Holmes, R.D. Levin, W.G. Mallard, Gas-Phase Ion and Neutral Thermochemistry, J. Phys. Chem. Ref. Data, vol. 17, 1988.
[25] J.R. Pliego, W.B. DeAlmeida, J. Chem. Soc., Faraday Trans. 93 (1997) 1881.
[26] Acidities of MCP^+ and VA^+ were calculated at the B3LYP/6-311G(d,p) level as $\Delta H_{r,0}$ for the reactions $C_4H_4^+ \rightarrow C_4H_3 + H^+$. Zero point energy corrections were scaled by a factor of 0.9806 (Ref. [19]).
[27] A.A. Gamble, J.R. Gilbert, J.G. Tillett, Org. Mass Spectrom. 3 (1970) 1223.
[28] A.A. Gamble, J.R. Gilbert, J.G. Tillett, Org. Mass Spectrom. 5 (1971) 1093.
[29] H. Bosshardt, M. Hesse, Angew. Chem. 86 (1974) 256.
[30] P.C. Vijfhuizen, W. Heerma, G. Dijkstra, Org. Mass Spectrom. 10 (1975) 919.
[31] F.M. Benoit, A.G. Harrison, Org. Mass Spectrom. 11 (1976) 599.
[32] E.D. Hoffmann, V. Stroobant, Mass Spectrometry Principles and Applications, 2nd ed., John Wiley & Sons, Ltd., Chichester, England, 2002.
[33] E. Gridelet, R. Locht, A.J. Lorquet, J.C. Lorquet, B. Leyh, J. Phys. Chem. A 112 (2008) 10086.

[34] C. Gonzales, H.B. Schlegel, J. Chem. Phys. 90 (1989) 2154.
[35] A series of constrained optimizations was performed in which the R(N-C_3) distance (see Fig. 7a) was held fixed at values ranging from 7.0 to 3.5 angstroms, in intervals of $\Delta R = 0.5$, while the remaining geometrical degrees of freedom were fully optimized. The corresponding total energies monotonically decrease with decreasing R(N-C_3) (see Fig. S1 in the Supplementary Information), thereby suggesting that intermediate I-0 forms from separated reactants without a barrier.
[36] The R(N-C_2) distance (see Fig. 7b) was held fixed at values ranging from 1.5 angstroms (close to the fully optimized N-C_2 bond length of 1.492 angstroms in I-1) to 3.1 angstroms (near the fully optimized N-C_2 distance of 3.208 in I-0), in increments of $\Delta R = 0.1$, while the remaining geometrical degrees of freedom were fully optimized. The corresponding total energies monotonically increase with increasing R(N-C_2) (see Fig. S2 in the Supplementary Information), with the constrained structure with R(N-C_2) fixed at 3.1 angstroms being 0.6 kcal/mol more stable than I-0. The similarity in geometry and energy between I-0 and the constrained structure with R(N-C_2) fixed at 3.1 angstroms (see Fig. S2) suggests that the presumed transition state TS-0,1 is only slightly higher in energy than I-0.
[37] P. Valtazanos, K. Ruedenberg, Theor. Chim. Acta 69 (1986) 281.
[38] A geometry optimization was performed starting from TS-4,4, in which the initial geometry step in the optimization was taken along the direction of the transition vector. The optimization converged to I-4, which suggests that the actual minimum energy path from TS-4,4 leads to I-4.